FULL PAPER

Dalton
www.rsc.org/dalton

On the electronic structure and spectroscopic properties of a pseudo-tetrahedral cationic cobalt(II) tetraamine complex – ([3^5]adamanzane)cobalt(II) †

Peter W. Thulstrup, Louise Broge, Erik Larsen and Johan Springborg
Chemistry Department, Royal Veterinary and Agricultural University, Thorvaldsensvej 40, DK-1871 Frederiksberg C, Denmark. E-mail: josp@kvl.dk

Received 21st May 2003, Accepted 9th June 2003
First published as an Advance Article on the web 7th July 2003

The electronic structure and spectrum of the unusual pseudo-tetrahedral cobalt(II) coordination compound formed with the bicyclic tetraamine ligand 1,5,9,13-tetraazabicyclo[7.7.3]nonadecane ([3^5]adz) has been investigated. The ligand-field absorption spectrum of the quartet ground state of the $[Co([3^5]adz)]^{2+}$ cation was resolved into five components, which were assigned by application of angular overlap model (AOM) calculations. Furthermore, density functional theory (DFT) and time-dependent DFT (TD-DFT) were applied to investigate the structure and absorption spectrum of the cation using the B3LYP functional in combination with various basis sets. The DFT calculations provided a geometry for the cation in excellent agreement with the crystal structure of $[Co([3^5]adz)]ZnCl_4$. The theoretical investigation of the electronic spectrum of the cation shows that TD-DFT can successfully be applied to open shell transition metal compounds, although only spin-allowed, single electron transitions are accounted for.

Introduction

Macrocyclic ligands are used in coordination chemistry as an attractive vehicle for trapping transition metal ions in unusual environments. It is of obvious interest to mimic the structure and function of the metal centers in the active sites of biological macromolecules, in a stable and easily manipulated system. Bi- and tricyclic tetraamines, known as adamanzanes, are examples of a class of ligands, which can be used to bind transition metal ions in a variety of coordination geometries, as described in a recent article.[1] In the present paper we examine the unusual cationic cobalt(II) compound formed with the bicyclic adamanzane ligand, 1,5,9,13-tetraazabicyclo[7.7.3]-nonadecane. This so-called bowl adamanzane, abbreviated as [3^5]adz,[1,2] is shown in Fig. 1.

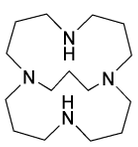

Fig. 1 [3^5]adz, 1,5,9,13-tetraazabicyclo[7.7.3]nonadecane.

The pink tetrachlorozincate salt of the $[Co([3^5]adz)]^{2+}$ cation was previously characterized by X-ray crystallography, and the cobalt(II) ion was found to be four-coordinated in a pseudo-tetrahedral geometry.[3] The crystalline product was isolated from a pink aqueous solution, indicating that the tetrahedral coordination of cobalt(II) is also the prevalent in solution. Cobalt(II) is well-known for its ability to form tetrahedral coordination compounds, such as the intensely blue tetrachlorocobaltate(II) anion. While cobalt(II) has a strong tendency to form high-spin tetrahedral complexes with weak field ligands, a more diverse situation is seen for the four-coordinate complexes of stronger field ligands. Here, the resulting compounds may also be low-spin square planar complexes,[4] and recently even a low-spin tetrahedral cobalt(II) complex has been reported.[5] Tetrahedral complexes of cobalt(II) with amine ligands are quite rare. The few examples found in the literature are tetraammincobalt(II) perrhenate,[6] the tetrahedral cobalt(II) species found in neat solution of some organic amines[7] and cobalt(II) complexes of the 16-membered ligands 1,5,9,13-tetraazacyclohexadecane ([16]aneN$_4$)[8] and 2,4,4,10,12,12-hexamethyl-1,5,9,13-tetraazacyclohexadecane (Me$_6$[16]aneN$_4$).[9] The latter compound and the $[Co([3^5]adz)]^{2+}$ ion are unique examples of tetrahedral Co(II) amine complexes, which resist oxidation to cobalt(III) in aqueous solution.

In this study an investigation of the electronic structure and spectroscopic properties of the $[Co([3^5]adz)]^{2+}$ ion is presented. Ligand-field theoretical calculations were carried out using the Angular Overlap Model (AOM) with respect to the ordering of the quartet states for the cobalt(II) ion in the pseudo-tetrahedral geometry. Density functional theory (DFT) calculations were applied to the study of the gas-phase geometry and electronic absorption spectra of the $[Co([3^5]adz)]^{2+}$ complex.

Through the last decade DFT has been widely and successfully applied to study electronic ground-state properties of coordination compounds, but so far it has been problematic to deal with excited states using DFT.[10] A promising method for the prediction of electronic absorption spectra has been found in the time-dependent DFT (TD-DFT) approach.[10,11] TD-DFT has been applied in numerous cases to organic molecules, including both closed-[12,13] and open-shell organic species.[14] Some examples of applications of TD-DFT to inorganic compounds have also been reported,[15] but only a few have dealt with open-shell species.[16] A recent study discusses the difficulty in treating species where two-electron transitions occur.[17] In the present article TD-DFT is used to study the spin-allowed electronic transitions for the quartet ground state of the $[Co([3^5]adz)]^{2+}$ ion.

Experimental

Abbreviations and nomenclature

The simplified nomenclature suggested for adamanzanes has been discussed recently.[1,2] For example, the IUPAC recommended name for $[Co([3^5]adz)](PF_6)_2$, is (1,5,9,13-tetraazabicyclo[7.7.3]nonadecane) cobalt(II) dihexafluorophosphate.

† Electronic supplementary information (ESI) available: Table S1: Cartesian coordinates of the DFT optimized geometry of the $[Co([3^5]adz)]^{2+}$ ion. Table S2: Results of experimental and calculated infrared absorption spectra for the $[Co([3^5]adz)]^{2+}$ ion. See http://www.rsc.org/suppdata/dt/b3/b305712g/

DOI: 10.1039/b305712g

Materials

$[Co([3^5]adz)](PF_6)_2$ and $[Co([3^5]adz)]ZnCl_4$ were prepared by published methods.[3] All other chemicals were of analytical grade.

Calculations

Multipeak Gausian analysis was performed using the program Origin.[18] Ligand-field calculations were made using the program LIGFIELD, version 0.91.[19]

Spectral measurements

A Cary 3 spectrophotometer was used for spectral measurements in the ultraviolet and visible region 15000–50000 cm^{-1} and a Zeiss DMR 21 spectrophotometer was used for spectral measurements in the 6250–15000 cm^{-1} region. The absorption spectra were measured at 2–3 °C using freshly prepared solutions of $[Co([3^5]adz)](PF_6)_2$ in 0.01 M CF_3SO_3H within minutes after their preparation. IR absorption spectra were obtained on a Perkin-Elmer 2000 FT-IR spectrophotometer operated in the mid-IR region (400–4000 cm^{-1}) using a KBr beamsplitter and a standard TGS detector. Samples were prepared as KBr pellets, and background corrected spectra were taken as an average of 20 scans with a spectral resolution of 4 cm^{-1}.

Magnetic measurements

The magnetic moment was measured with a Faraday balance described elsewhere.[20] The measurements were performed at a field strength of 1.35 T in the temperature range 4.5–300 K. The data were corrected using Pascal's constants.

Density functional theoretical calculations

A series of gas-phase calculations using Density Functional Theory (DFT) and time-dependent DFT (TD-DFT) were carried out on the $[Co([3^5]adz)]^{2+}$ complex with a quartet ground state. The geometry was optimized starting from the published coordinates of the crystal structure.[3] Initial calculations were performed within the C_2 point group using the spin-unrestricted formalism and the B3LYP hybrid functional[21] and the 3-21G* basis set. B3LYP was the only DFT functional that was used in the investigation. All calculations were performed using Gaussian 98[22] on either a dual-Pentium Linux PC running Gaussian 98 Rev A7 or on a Sun Fire supercomputer running Gaussian 98 Rev A11. The final geometry was achieved using the TZV basis set of Ahlrichs.[23] At this level of theory there were 392 basis functions (788 primitive gaussians) for the 89 α and 86 β electrons. The final SCF energy was 2192.24887544 a.u. with an S^2 value of 3.7563 before and 3.7500 after annihilation of spin contamination. The ^4A wave function was confirmed to be the ground state by stability analysis. A frequency calculation was performed to confirm that the stationary state was a true minimum, and the results were used for comparison with the infrared absorption spectrum. Raman intensities were not computed. For the TD-DFT calculations the geometry obtained with the TZV basis set was used in TD-UB3LYP calculations with the basis sets: 6-31G**, 6-31++G**, 6-311G**, 6-311++G**, TZV, and TZVP, as these are implemented in the Gaussian 98 program.

Results and discussion

Ligand-field spectrum and calculations

The magnetic moment of $[Co([3^5]adz)](PF_6)_2$ is 4.2 μ_B at 300 K, 4.1 μ_B at 10 K and then the magnetic moment decreases sharply at further decrease in the temperature. This behavior follows the expectations for a tetrahedral cobalt(II) complex with a quartet ground state. The solution ligand-field spectrum of $[Co([3^5]adz)](PF_6)_2$ (0.01 M CF_3SO_3H, 2–3 °C) shown in Fig. 2 was resolved into five components. The shape of the band centered at 18400 cm^{-1} is not gaussian, and attempts to resolve it into gaussian components failed. Therefore, this part of the spectrum was kept as a single band while the spectrum between 6,250 cm^{-1} and 15,000 cm^{-1} was resolved into gaussians. The optimal resolution was obtained using four gaussian components, which reproduce excellently this part of the observed spectrum as shown in Fig. 2. The ultraviolet absorption spectrum revealed a single absorption band, centered at 43000 cm^{-1} (ε = 1400 M^{-1} cm^{-1}) with a tail of absorption extending to 28000 cm^{-1} (data not shown).

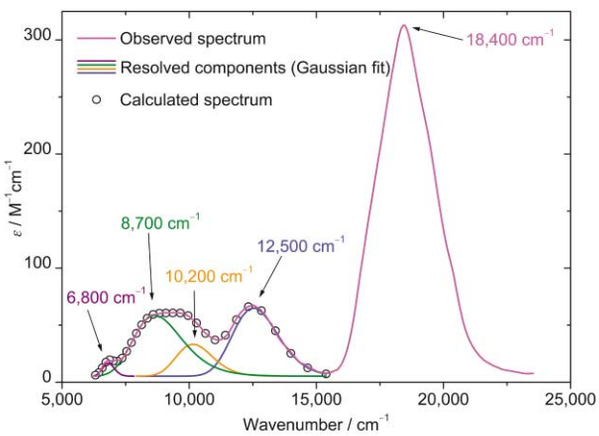

Fig. 2 Visible and near infrared absorption spectrum of $[Co([3^5]adz)](PF_6)_2$ in 0.01 M CF_3SO_3H measured at 2–3 °C. The observed spectrum is in the region 6250 cm^{-1}–15000 cm^{-1} reproduced excellently by four gaussian components. The sum of the gaussian curves overlap the observed curve.

The five observed absorption bands in the ligand-field region were assumed to be fully of d–d origin and then used to fit ligand-field and electronic repulsion parameters within the Angular Overlap Model (AOM).[24] Spin-orbit coupling was not included in these calculations. Since no spin-forbidden transitions were observed the electronic repulsion parameters B and C cannot be determined independently, and throughout the calculations the relation $C = 4B$ was assumed.

The crystal structure analysis shows that the cation has a pseudo-tetrahedral geometry with approximate C_{2v} symmetry and the N–Co–N angles thus deviate from the 109° corresponding to ideal tetrahedral geometry. The N_{tert}–Co–N_{tert} angle was found to be 104° and the N_{sec}–Co–N_{sec} angle was 125°. In the following calculations these angles from the crystal structure have been used, assuming that the structures of the cation in solution and in the solid are identical. This seems reasonable considering the inherent rigid property of the macrocyclic ligand.

The three spin-allowed transitions in a tetrahedral d^7 complex are from the ground state $^4A_2(F)$ to the excited states $^4T_2(F)$, $^4T_1(F)$ and $^4T_1(P)$. Deviation from tetrahedral geometry to approximate C_{2v} symmetry, as in the present complex, causes splitting of each of the three excited states into three non-degenerate states. These energy levels were first described by guessed values for e_σ and B in the actual geometry. Then the two parameters were fitted to the five experimentally obtained maxima for the gaussian components shown in Fig. 2, using the Leuwenberg–Marckardt method. The resulting energy levels are reported in Table 1. The calculated parameter values are e_σ = 5,251(249) cm^{-1} and B = 578(63) cm^{-1}.

The Walsh diagram based on these parameters is seen in Fig. 3. The energies of the nine non-degenerate states are shown as a function of the deviation from ideal tetrahedral geometry. This deviation is expressed as a gradual increase of the N_{sec}–Co–N_{sec} angle from 109 to 125° and a simultaneous gradual decrease of

Table 1 Observed and AOM calculated energy differences for the spin-allowed transitions for the $[Co([3^5]adz)]^{2+}$ complex with a $^4A_2(F)$ ground state. AOM parameters: $e_\sigma = 5251\ cm^{-1}$, $B = 578\ cm^{-1}$

Energy levels, symmetry labels and contributions from F and P terms (%)[a]						Energy differences/cm^{-1}		
T_d	F	P	C_{2v}	F	P	E_{calc}	E_{calc} (av.)	E_{obs}
$^4T_1(P)$	19	81	B_1	16	84	18 800	18 200	18 400
			A_2	7	93	18 000		
			B_2	38	62	17 900		
$^4T_1(F)$	81	19	B_2	63	37	13 200	13 200	12 500
			A_2	94	6	11 100	11 100	10 200
$^4T_2(F)$	100	0	B_1	86	14	9 200	8 700	8 700
			A_1	100	0	8 200		
			B_2	97	3	6 200	5 800	6 800
			B_1	99	1	5 300		
$^4A_2(F)$	100	0	A_2	99	1	0	0	–

[a] If spin-orbit coupling ($\zeta = 490\ cm^{-1}$)[25] is included in the calculations for T_d symmetry, the $^4T_1(P)$ states contain 22–59% F character, 40% on average.

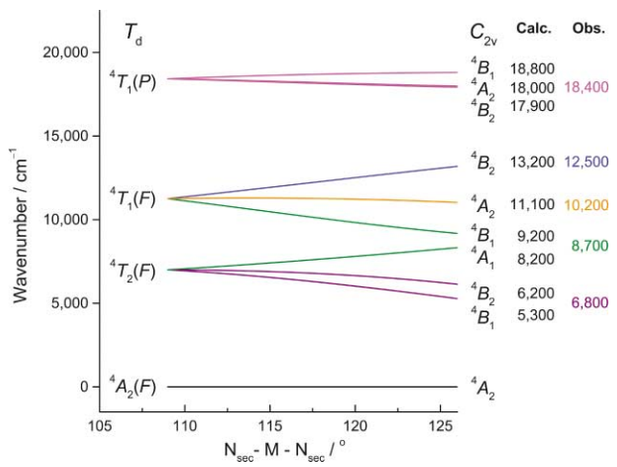

Fig. 3 Walsh diagram showing the energy as a function of the N_{sec}–Co–N_{sec} angle, which is gradually changed from 109 to 125° (with a simultaneous gradual decrease of the N_{tert}–Co–N_{tert} angle from 109 to 104°). Also noted are the symmetry labels of the states in the T_d and C_{2v} point groups. AOM parameters: $e_\sigma = 5{,}251\ cm^{-1}$, $B = 578\ cm^{-1}$.

the N_{tert}–Co–N_{tert} angle from 109 to 104°. As is seen from the Walsh diagram (Fig. 3) the energy levels for the actual N–Co–N angles in the present compound are grouped in five regions corresponding to the observed five components in the absorption spectrum, and the final calculations were based upon assignments according to this result.

The AOM calculations also reveal the contributions from the atomic F and P terms to the energy levels of the $[Co([3^5]adz)]^{2+}$ ion. The calculations were performed for T_d and C_{2v} symmetry, and the contributions are given as percentages in Table 1. The states of T_2 heritage are of pure F character for T_d symmetry and practically pure F character for C_{2v} symmetry. The T_1 states, however, mix to some extent. In T_d symmetry an admix of 20% P character into the $^4T_1(F)$ term is seen. Correspondingly the $^4T_1(P)$ contains a 20% contribution from functions of F character. On average, the situation is similar in C_{2v} symmetry. However, the B_2 states account for the major part of the mixing (*ca.* 38%) whereas the B_1 and A_2 states have only minor contributions.

AOM calculations on the $CoCl_4^{2-}$ ion have been reported, and they revealed a very different situation.[25] A much larger degree of mixing is present for this system, and the $T_1(P)$ term was actually reported to contain 60–70% F character. This result was supported by *ab initio* calculations.[26] However, spin-orbit coupling was included for the $CoCl_4^{2-}$ calculations. If a fixed spin-orbit coupling parameter, $\zeta = 490\ cm^{-1}$, is included in the $[Co([3^5]adz)]^{2+}$ AOM calculations using T_d symmetry and $e_\sigma = 5251\ cm^{-1}$ and $B = 578\ cm^{-1}$ the F contributions to the $^4T_1(P)$ states lie in the range 22–59%, averaging to 40%. This fact explains the intensity of the absorption band assigned to the transition to the $^4T_1(P)$ state (Fig. 2). However, only a minor effect on the *energies* of the various states is seen upon such an inclusion of the spin-orbit coupling. This justifies leaving ζ out for reasons of simplicity of the calculations for the Walsh diagram and the fitting procedure for the e_σ and B parameters.

Table 2 Bond lengths (Å) and angles (°) for cobalt from the gas-phase DFT (UB3LYP/TZV) geometry for the $[Co([3^5]adz)]^{2+}$ ion. Averages of experimental values are given for the crystal structure of $[Co([3^5]adz)][ZnCl_4]$.[3]

	UB3LYP/TZV	Crystal structure
N_{sec}–Co	2.044	2.008
N_{tert}–Co	2.036	2.022
N_{sec}–Co–N_{sec}	123.53	126.22
N_{tert}–Co–N_{sec}	105.80	104.71
N_{sec}–Co–N_{tert}	107.23	107.52
N_{tert}–Co–N_{tert}	106.15	104.31

The full spectral data for the pseudo-tetrahedral $[Co(NH_3)_4]^{2+}$, $[Co(H_2NPr)_4]^{2+}$, $[Co([16]aneN_4)]^{2+}$ and $[Co(Me_6[16]aneN_4)]^{2+}$ ions are not available, rendering ligand-field comparisons impossible. However, the main d–d absorption bands for these complexes all lie in the region 17 500–20 000 cm^{-1},[6–9] placing the $[Co([3^5]adz)]^{2+}$ complex in the middle with regards to ligand-field strength (main absorption band at 18 400 cm^{-1}).

Density functional theory

Whereas the AOM results only consider the interaction of cobalt(II) with four coordinating nitrogen atoms, the present DFT treatment involves the entire ligand in the $[Co([3^5]adz)]^{2+}$ complex. It is of interest to evaluate how well the geometry and vibrational frequencies of this large system are predicted, even though only solid phase experimental data are available for comparison. In Table 2 the important structural parameters concerning the cobalt(II)–nitrogen bonds are given for the gas-phase DFT calculation and the experimental crystal structure.[3]

The table shows that the DFT Co–N bond lengths are within 0.04 Å of the experimental values, both being very close to 2.0 Å. The distorted tetrahedral geometry of the cation found in the crystal structure of the tetrachlorozincate salt, is also well reproduced by gas-phase DFT calculations. The largest divergence of 2.7° is found in the unusually wide tetrahedral angle between the secondary amine nitrogen atoms. The geometry of the cation in the crystal is affected by a hydrogen-bonding interaction between the tetrachlorozincate anion and the amine hydrogens with H–Cl distances of *ca.* 2.4 Å. The structural DFT parameters for the ligand were found to be in satisfactory agreement with the crystal data as illustrated in Fig. 4.

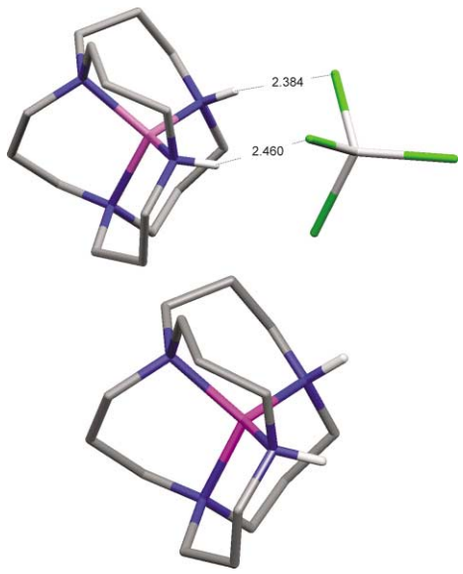

Fig. 4 Top: Illustration of the experimental crystal structure of $[Co([3^5]adz)]ZnCl_4$ from ref. 3 showing the hydrogen bonding between the amine hydrogens and the anion. H-bond distances are given in Å. Bottom: Rendering of the gas-phase geometry of the $[Co([3^5]adz)]^{2+}$ ion predicted by a UB3LYP/TZV DFT calculation. Cobalt is pink, nitrogen blue, carbon grey, chloride green, and zinc light grey. C–H hydrogen atoms have been omitted for clarity.

The Cartesian coordinates of the optimized theoretical geometry are listed in Table S1 (ESI †).

The vibrational spectra of the cation were investigated to further establish that the gas-phase DFT calculations provide a valid model to interpret solid and solution phase experimental data. The IR-active frequencies predicted by the UB3LYP/TZV gas phase calculation were compared to experimental FT-IR spectra of KBr pellets of $[Co([3^5]adz)]ZnCl_4$ and $[Co([3^5]adz)](PF_6)_2$, and the results are shown in Fig. 5. The IR spectra are highly composite arising from a total of 150 fundamental normal modes, distributed equally among the A and B irreducible representations in the C_2 point group. The micro-crystalline environment of the experimental spectra gives rise to broad, overlapping absorption bands, making it problematic to assign the bands to individual transitions. The agreement between calculation and experiment is clearly evident by visual inspection

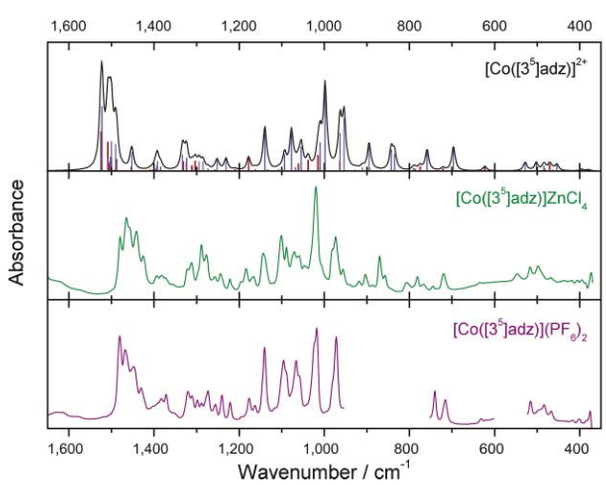

Fig. 5 IR Vibrational spectra of the $[Co([3^5]adz)]^{2+}$ ion. Top: Unscaled harmonic frequencies predicted for the $[Co([3^5]adz)]^{2+}$ ion from a UB3LYP/TZV calculation. Only the IR active vibrations in the mid-IR region are shown, where red and blue columns represent vibrations of A and B symmetry within the C_2 point group, respectively. The black curve is a simulated spectrum (lorenzian lineshape with FWHH = 5 cm^{-1}) allowing for comparison with experimental data. Middle and bottom: Experimental FT-IR absorption spectra (KBr pellets) of $[Co([3^5]adz)]ZnCl_4$ and $[Co([3^5]adz)](PF_6)_2$, respectively.

of the three curves presented in Fig. 5. The displacement of the calculated frequencies relative to the experimental signals is particularly evident at higher frequencies. This is a well-known shortcoming of the density functional treatment, and the scaling factor is in agreement with previously published values.[27] The Co–N stretching vibrations are observed in the 400–500 cm^{-1} range. The bulk of the observed IR absorption bands can be assigned to the vibrations of the organic ligand. A complete listing of the computed vibrational data is given in Table S2 (ESI †), including tentative assignments of the experimental spectra based on frequency and intensity criteria.

The spin-allowed electronic transitions of the $[Co([3^5]adz)]^{2+}$ complex were calculated using TD-DFT. It is of considerable interest to evaluate how well TD-DFT can describe the electronic spectra of open-shell transition metal complexes. In the case of the $[Co([3^5]adz)]^{2+}$ ion, application of TD-DFT is especially relevant, because the size of the molecule makes a theoretical treatment at a higher level extremely demanding. Furthermore, the non-degenerate $^4A_2(F)$ ground state should be well described by a Kohn–Sham wavefunction. However, one major shortcoming of the applied TD-DFT treatment should be noted; namely that the double excitations into the states derived from the $^4T_1(P)$ state are not accessible. Initially, it is instructive to consider the ordering of the Kohn–Sham orbitals of d-character, which are illustrated in Fig. 6. The five highest occupied α orbitals have both ligand and metal contributions, but the e set (z^2, x^2-y^2) and the t_2 set (zx, yz, xy) can easily be identified. The β orbitals illustrated in Fig. 6 are of pure d-character, with the e set being the highest occupied β orbitals, and the t_2 set being the lowest virtual orbitals. Thus, with respect to the nature of d-orbitals the DFT description of the electronic structure is in agreement with the AOM treatment, and the Kohn–Sham orbitals of d-character are denoted with reference to the atomic d-functions (z^2, x^2-y^2, zx, yz, xy). In Table 3 the results of TD-UB3LYP calculations for a number of basis sets are given for the ten lowest excited states of the $[Co([3^5]adz)]^{2+}$ complex.

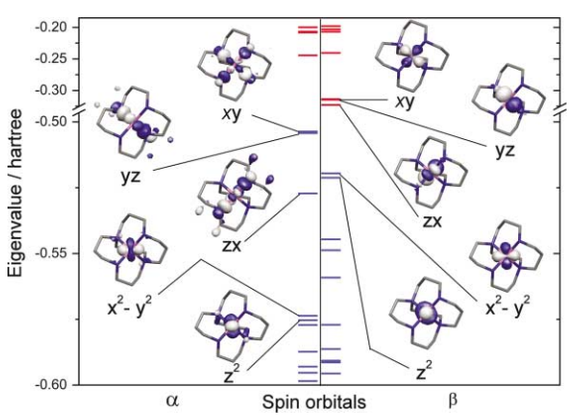

Fig. 6 A plot of the eigenvalues (Hartree) of the valence Kohn–Sham orbitals from a UB3LYP/TZV calculation for the $[Co([3^5]adz)]^{2+}$ ion. The horizontal bars represent α and β spin-orbitals, shown to the left and right, respectively. Blue bars represent occupied orbitals and red bars represent virtual orbitals. The five highest occupied α spin-orbitals are illustrated to the left, while the two highest occupied and three lowest virtual β spin-orbitals are shown to the right.

For all six of the tested basis sets the TD-DFT results are quite similar with respect to the nature of the excited states. The ten lowest excitations involve only β spin-orbitals, and the ordering of the states is the same for all basis sets. The six lowest excited states are of d–d character, and the leading configurations contributing to the transitions are indicated in Table 3 by indication of the respective d-orbital labels. These six states correspond to three excited states of $^4T_2(F)$ heritage and three excited states of $^4T_1(F)$ heritage. All six d–d transitions can thus be interpreted as involving the promotion of a single electron

Table 3 Results from TD-UB3LYP calculations on the $[Co([35]adz)]^{2+}$ ion with various basis sets. The lowest ten excited states are given with their respective irreducible representations in the C_2 point group indicated. Transition energies (rounded to 100 cm^{-1}) are given as wavenumbers/cm^{-1}, and the computed oscillator strengths are given in parentheses. The excited states are described in terms of the nature of the Kohn–Sham orbitals involved in the leading configurations. To the far right, the corresponding maxima of the resolved absorption bands from the electronic spectrum are given.

Excited state	6-31G**	TZV	6-31++G**	6-311++G**	TZVP	6-311G**	Description	$\tilde{\nu}_{max}$/cm^{-1}
State 1 (B)	6700 (0.0000)	7300 (0.0000)	7400 (0.0000)	7500 (0.0000)	7500 (0.0000)	7600 (0.0000)	$z^2 \longrightarrow zx$ $x^2-y^2 \longrightarrow zx$	6800
State 2 (B)	8000 (0.0000)	8600 (0.0001)	8800 (0.0001)	8800 (0.0001)	8900 (0.0001)	9200 (0.0001)	$z^2 \longrightarrow yz$ $x^2-y^2 \longrightarrow zx$	
State 3 (A)	9300 (0.0000)	9800 (0.0000)	10100 (0.0000)	10100 (0.0000)	10100 (0.0000)	10400 (0.0000)	$x^2-y^2 \longrightarrow xy$	8700
State 4 (B)	13200 (0.0017)	13400 (0.0018)	13500 (0.0020)	13500 (0.0020)	13600 (0.0020)	14000 (0.0019)	$z^2 \longrightarrow yz$ $x^2-y^2 \longrightarrow zx$	
State 5 (B)	14800 (0.0022)	15100 (0.0023)	15300 (0.0026)	15300 (0.0026)	15400 (0.0025)	16000 (0.0024)	$x^2-y^2 \longrightarrow yz$ $z^2 \longrightarrow zx$	10200
State 6 (A)	15700 (0.0015)	16200 (0.0017)	16300 (0.0019)	16300 (0.0018)	16400 (0.0018)	16700 (0.0016)	$z^2 \longrightarrow xy$	12500
State 7 (A)	38700 (0.0000)	36300 (0.0000)	35400 (0.0000)	35600 (0.0000)	35500 (0.0000)	37200 (0.0000)	LMCT	43000
State 8 (B)	39500 (0.0055)	37200 (0.0070)	36300 (0.0068)	36400 (0.0067)	36300 (0.0072)	38100 (0.0079)	LMCT	
State 9 (B)	40900 (0.0124)	38700 (0.0137)	37900 (0.0134)	38000 (0.0133)	37900 (0.0148)	39800 (0.0210)	LMCT	
State 10 (A)	41100 (0.0053)	38900 (0.0064)	38000 (0.0069)	38100 (0.0067)	38100 (0.0068)	40300 (0.0071)	LMCT	

from an e orbital to a t_2 orbital. The three first excited states are all predicted to have oscillator strengths close to zero. The next three predicted d–d transitions in Table 3 are predicted to have higher intensity, which is in agreement with the experimental findings (Fig. 2). The first two lowest transitions with a B representation are very similar in nature, both involving a single electron transition of the type $z^2/x^2-y^2 \longrightarrow zx/yz$, with reference to the orbitals illustrated in Fig. 6. The first absorption band observed at 6800 cm^{-1} is assigned to these two transitions. The third transition of Table 3 can be interpreted as a $x^2-y^2 \longrightarrow xy$ transition. The second observed absorption band at 8700 cm^{-1} is assigned to the third and fourth transitions, the fourth transition having the largest predicted intensity. The absorption band observed at 10200 cm^{-1} is assigned to the fifth transition of the $z^2/x^2-y^2 \longrightarrow zx/yz$ type, while the band at 12500 cm^{-1} is assigned to the sixth transition having $x^2-y^2 \longrightarrow xy$ character. The strong absorption band observed at *ca.* 18400 cm^{-1} has not been assigned here, since the three states of $^4T_1(P)$ heritage are not predicted by TD-DFT. The excited states labelled 7–10 in Table 3, are all of ligand to metal charge transfer (LMCT) character involving charge migration from nitrogen to cobalt. The allowed LMCT transitions are 5–10 times more intense than the strongest d–d transition, which agrees well with the experimental findings (d–d band at 18400 cm^{-1}, ε = 300 M^{-1} cm^{-1}, UV band at 43000 cm^{-1}, ε = 1400 M^{-1} cm^{-1}).

The spread in excitation energies and oscillator strengths indicated in Table 3 is surprisingly small considering that both double and triple zeta basis sets with and without diffuse functions have been tested. If the LMCT transitions are considered, it is clear from Table 3 that in particular the 6-31G** and 6-311G** values are higher in energy, than the values obtained with the other basis sets. The values for the TZV calculation are also somewhat higher than the values for 6-31++G**, 6-311++G**, and TZVP which have values that are very close to each other. The results obtained for the large basis sets are also closest to the observed absorption maximum at 43000 cm^{-1}. Thus, for the LMCT transitions the 6-31++G**, 6-311++G**, and TZVP basis sets provide approximately equal results. Seemingly, it is more important to include diffuse functions rather than to increase basis set size to triple zeta quality, although the TZV also does perform rather well even without additional polarization or diffuse functions. In previous investigations using TD-DFT it is often stressed that the inclusion of diffuse functions is essential for a proper treatment of excited states involving higher lying virtuals, such as Rydberg states.[12]

If the transition energies for the lowest six transitions are compared to the experimental absorption maxima, the trend seen for the LMCT transitions is also evident here. The transition energies for 6-31++G**, 6-311++G**, and TZVP are practically identical, with the TZV basis set predicting slightly lower transition energies for the six d–d transitions. The 6-31G** and 6-311G** basis sets produce the values that deviate the most from the values obtained with other four basis sets, being lower in energy for 6-31G** and higher in energy for 6-311G**. It is notable that the 6-31G**, *i.e.* the smallest basis set tested, produces the values which are closest to the experimental transition energies for the d–d transitions.

Closer inspection of Table 3 clearly shows that the experimental transition energies are considerably lower than the values predicted by TD-DFT for the d–d transitions, while the opposite is true for the LMCT transitions. The first three transitions are reasonably well described in terms of excitation energy, but the results for the next three transitions are rather poor. This is probably a consequence of the inability of TD-DFT to account for the coupling that occurs between the states of $^4T_1(F)$ and $^4T_1(P)$ heritage (Table 1). It has previously been noted that pure two-electron transitions are not accessible using TD-DFT. However, the energies of one-electron transitions having substantial double excitation character are predicted as well as pure one-electron transitions.[17]

The average deviation between theory and experiment for the six basis sets is *ca.* 1200 cm^{-1} for the first three transitions and *ca*. 4100 cm^{-1} for the following three transitions, giving an average deviation of *ca.* 2650 cm^{-1} for all six d–d transitions. These deviations are within the range of 0.1 to 1.0 eV, reported for TD-DFT previously.[11–17] Although this numerical deviation is larger than is the case for the AOM calculations the two methods correspond well with regards to the general pattern of the excited states and the splitting caused by the distortion of the $Co([3^5]adz)^{2+}$ complex from ideal tetrahedral symmetry.

Conclusion

The results show that TD-DFT may efficiently provide valuable information for extensive systems. A careful interpretation of the results is needed, however, as the TD-DFT methodology cannot take formal two-electron excitations into account. It is illustrated how a combination of density functional theory computation with empirical ligand-field theory is valuable for a full understanding and assignment of transitions in coordination compounds, notably when double excitation takes place.

Acknowledgements

E. L. and P. W. T. acknowledge DCSC grant CPU-1101–31 for supercomputer CPU resources. The magnetic susceptibility measurements were kindly provided by J. Glerup, H.C. Ørsted Institute, University of Copenhagen. E. L. wishes to acknowledge membership of the COST D21.007 working group.

References

1 J. Springborg, *Dalton Trans.*, 2003, 1653.
2 J. Springborg, C. E. Olsen and I. Søtofte, *Acta Chem. Scand.*, 1995, **49**, 555.
3 L. Broge, U. Pretzmann, N. Jensen, I. Søtofte, C. E. Olsen and J. Springborg, *Inorg. Chem.*, 2001, **40**, 2323.
4 G. W. Everett Jr. and R. H. Holm, *Inorg. Chem.*, 1968, **7**, 776.
5 D. M. Jenkins, A. J. Di Bilio, M. J. Allen, T. A. Betley and J. C. Peters, *J. Am. Chem. Soc.*, 2002, **124**, 15336.
6 H. V. A. Briscoe, P. L. Robinson and A. J. Rudge, *J. Chem. Soc.*, 1931, 2211; A. Müller, P. Christophliemk and I. Tossidis, *J. Mol. Struct.*, 1973, **15**, 289.
7 S. Aizawa, S. Iida, K. Matsuda and S. Funahashi, *Inorg. Chem.*, 1996, **35**, 1338.
8 L. Chen and F. A. Cotton, *Inorg. Chim. Acta*, 1997, **263**, 9.
9 N. F. Curtis and O. P. Gladkikh, *Aust. J. Chem.*, 2000, **53**, 727.
10 W. Koch and M. C. Holthausen, *A chemist's guide to density functional theory*, Wiley-VCH, Weinheim, 2000.
11 R. E. Stratmann, G. E. Scuseria and M. J. Frisch, *J. Chem. Phys.*, 1998, **109**, 8218.
12 K. B. Wiberg, R. E. Stratmann and M. J. Frisch, *Chem. Phys. Lett.*, 1998, **297**, 60.
13 J. Fabian, *Theor. Chem. Acc.*, 2001, **106**, 199; L. E. Forslund, R. Faust and N. Kaltsoyannis, *J. Chem. Soc., Perkin Trans. 2*, 2002, 494.
14 S. Hirata and M. Head-Gordon, *Chem. Phys. Lett.*, 1999, **302**, 375; J. Guan, M. E. Casida and D. R. Salahub, *J. Mol. Struct. (THEOCHEM)*, 2000, **527**, 229.
15 S. I. Gorelsky and A. B. P. Lever, *J. Organomet. Chem.*, 2001, **635**, 187; S. J. A. van Gisbergen, J. A. Groenewald, A. Rosa, J. G. Snijders and E. J. Baerends, *J. Phys. Chem. A*, 1999, **103**, 6835.
16 E. Broclawik and T. Borowski, *Chem. Phys. Lett.*, 2001, **339**, 433; T. Borowski, M. Krol, M. Chruszcz and E. Broclawik, *J. Phys. Chem. B*, 2001, **105**, 12212.
17 D. J. Tozer, R. D. Amos, N. C. Handy, B. O. Roos and L. Serrano-Andres, *Mol. Phys.*, 1999, **97**, 859.
18 Origin Professional, version 5.0; Microcal Software, Inc., Northampton, MA, 1997.
19 J. Bendix: LIGFIELD: An Extensive Program Package for Ligand Field Calculations on a PC, Proceedings of the 29th ICCC, Lausanne, Switzerland, 1992.
20 J. Josephsen and E. Pedersen, *Inorg. Chem.*, 1997, **16**, 2534.
21 A. D. Becke, *J. Chem. Phys.*, 1993, **98**, 5648.
22 M. J. Frisch, G. W. Trucks, H. B. Schlegel, G. E. Scuseria, M. A. Robb, J. R. Cheeseman, V. G. Zakrzewski, J. A. Montgomery, Jr., R. E. Stratmann, J. C. Burant, S. Dapprich, J. M. Millam, A. D. Daniels, K. N. Kudin, M. C. Strain, O. Farkas, J. Tomasi, V. Barone, M. Cossi, R. Cammi, B. Mennucci, C. Pomelli, C. Adamo, S. Clifford, J. Ochterski, G. A. Petersson, P. Y. Ayala, Q. Cui, K. Morokuma, D. K. Malick, A. D. Rabuck, K. Raghavachari, J. B. Foresman, J. Cioslowski, J. V. Ortiz, B. B. Stefanov, G. Liu, A. Liashenko, P. Piskorz, I. Komaromi, R. Gomperts, R. L. Martin, D. J. Fox, T. Keith, M. A. Al-Laham, C. Y. Peng, A. Nanayakkara, C. Gonzalez, M. Challacombe, P. M. W. Gill, B. G. Johnson, W. Chen, M. W. Wong, J. L. Andres, M. Head-Gordon, E. S. Replogle and J. A. Pople, GAUSSIAN 98 (Revision A.7), Gaussian, Inc., Pittsburgh, PA, 1998.
23 A. Schäefer, C. Huber and R. Ahlrichs, *J. Chem. Phys.*, 1994, **100**, 5829.
24 C. E. Schäffer, *Structure and Bonding*; Springer-Verlag, Berlin, Heidelberg, New York, 1968, vol. 5, p. 67; S. E. Harnung and C. E. Schäffer, *Struct. Bonding (Berlin)*, 1972, **12**, 257.
25 K. Kojima and J. Matsuda, *Bull. Chem. Soc. Jpn.*, 1986, **59**, 859.
26 H. Johansen and N. K. Andersen, *Mol. Phys.*, 1986, **58**, 965.
27 A. P. Scott and L. Radom, *J. Phys. Chem.*, 1996, **100**, 16502.